Chemical Vapor Deposition

DOI: 10.1002/cvde.201206988

Full Paper

Effect of AACVD Processing Parameters on the Growth of Greenockite (CdS) Thin Films using a Single-Source Cadmium Precursor**

By *Muhammad Ali Ehsan*, *Huang Nay Ming*, *Misni Misran*, *Zainudin Arifin*, *Edward R. T. Tiekink*, *Ahmad P. Safwan*, *Mehdi Ebadi*, *Wan J. Basirun*, and *Muhammad Mazhar**

Greenockite (CdS) nanostructured thin films are deposited on soda and FTO conducting glass substrates by aerosol-assisted (AA)CVD using a single-source precursor bis-(*N*,*N*-dicylcohexyldithiocarbamato)(pyridine)cadmium(II), $Cd[S_2CNCy_2]_2$.py (**1**), in pyridine, toluene, and THF solutions in the temperature range 350–450 °C. The precursor **1**, characterized by physicochemical methods, undergoes facile thermal decomposition at 350 °C to give a stable residual mass of CdS. The thin films deposited from pyridine solution, and characterized by X-ray diffraction (XRD), UV-vis spectroscopy, field-emission scanning electron microscopy (FESEM), and energy dispersive X-ray (EDX) techniques, exhibit a band gap of 2.4 eV and a photocurrent density of 1.3 mA cm^{-2} at 0.4 V versus Ag/AgCl/3M KCl, suggesting their suitability for application in photo-electrochemical (PEC) cells.

Keywords: Cadmium, Nanostructures, S-ligand, Thin films

1. Introduction

Cadmium sulfide (CdS) is probably the most investigated photoelectrode material, after TiO_2, because of its particular band gap of 2.4 eV[1] that enables the harvesting of most of the photons in the solar spectrum. Having met most of the stringent requirements for the ideal photocatalyst,[2] CdS however undergoes photo-corrosion and suffers from instability upon prolonged irradiation,[3] which mitigates its utility as a photoelectrode in photo-electrochemical water-splitting devices. Nevertheless, CdS still has many potential applications in optoelectronic materials, solar cells and photo-detectors, optical filters, multilayer light emitting diodes, flat panel display photodiodes, phototransistors, and window-layered heterojunction solar cells.[4,5] In view of the aforementioned applications, the investigation of new methods for the fabrication of nanoparticles, nanowires, and nanorods of CdS has been extensively conducted in recent years.[6,7] Several studies on the deposition of CdS thin films have been reported, including by electrodeposition,[8] chemical bath deposition,[9] spray pyrolysis techniques,[10] CVD,[11] vacuum evaporation methods,[12] and sputtering.[13] Since all of these methods suffer from high production costs, and often require complicated operations and instrumentation, work continues to explore more facile routes for the fabrication of CdS nanocrystallite thin films at low cost and in scalable ways.

The trend of using hazardous metal alkyls and H_2S for metal sulfide synthesis[14] is being replaced with a single-source molecular precursor approach because of potential advantages.[15] Various cadmium compounds have been reported as single-source precursors for the fabrication of thin films from CVD techniques, but later proved problematic because of their volatility, lack of stoichiometric control, and poor crystallinity of the target material.[15] One of the reasons for the volatility problem is that cadmium chalcogenides usually exist as high molecular weight polymeric complexes in which the metal centre is bridged by the chalcogenolato ligands to give pseudo-tetrahedral coordination at the metal ion,[16] thereby decreasing their value as precursors for metal-organic (MO)CVD applications. As a result, as observed in the past, most investigations on the formation of CdS thin films were made by low-pressure CVD using classes of cadmium molecular pre-

[*] Prof. M. Mazhar, M. A. Ehsan, Dr. M. Misran, Dr. Z. Arifin, Dr. E. R. T. Tiekink, A. P. Safwan, Dr. M. Ebadi, Dr. W. J. Basirun
Department of Chemistry, Faculty of Science,
University of Malaya Lembah Pantai,
50603 Kuala Lumpur (Malaysia)
E-mail: mazhar42pk@yahoo.com

Dr. H. N. Ming
Department of Physics, Faculty of Science,
University of Malaya Lembah Pantai,
50603 Kuala Lumpur (Malaysia)

Dr. M. Ebadi
Department of Chemistry,
Faculty of Sciences,
Islamic Azad University- Gorgan
Branch Gorgan (Iran)

[**] The Ministry of Higher Education (Malaysia) and the University of Malaya are thanked for funding this research through the High-Impact Research scheme (Grant numbers UM.C/625/1/HIR-C/035 and UM.C/HIR/MOHE/SC/03) and through the UMRG scheme (Grant number RG097/10AET).

 © 2012 WILEY-VCH Verlag GmbH & Co. KGaA, Weinheim

cursors and coordination complexes.[17] Low-pressure CVD usually operates under a vacuum of 10^{-2} Torr or lower, and has a few variables (such as substrate temperature or deposition time) to control the morphology and structure of the thin films. These stringent requirements and limitations have undermined the importance and applications of low-pressure CVD for thin film fabrication of CdS. The need for specifically tailored precursor molecules with adequate volatility for the deposition of nanocrystalline CdS thin films has grown with time. One approach for improving their performance as precursors is the addition of Lewis bases in order to decrease the degree of association present in the polymeric structure by forming monomeric complexes via the formation of adducts. Various dialkyldithiocarbamate cadmium (II) adducts, with mono and bidentate *N*,*N*′-donor bases, have been synthesized and reported previously but without exploring their capabilities as precursors for CVD.[18,19]

AACVD, a sub-class of CVD, relaxes the volatility restrictions thus allowing the use of a wide range of precursors to deposit multi-component layers, thereby ensuring both reproducibility and homogeneity in the deposited layer. The morphology and particle size of the deposit can be closely controlled by the choice of a suitable solvent, deposition temperature, and by controlling the frequency of the ultrasonic modulator. Several precursors, such as $[Cd(C_6H_{12}N_3S_2)_2]$,[18] $[Cd(C_{10}H_{20}N_3S_2)_2]$,[18] $Cd[(SP^iPr_2)_2N]_2$,[20] and $[Cd(C_{14}H_{28}N_3OS)_2]$,[21] have been employed for CdS thin film production by AACVD. All of these reports mainly focused on precursor engineering and produced the CdS phase at relatively high temperatures, with no appreciable control over the nanostructure of the thin films. The pursuit of well-defined nanostructures has been the target for many areas of applications, and is a central part of our research objective of employing them as solar water-splitting devices.[22,23] Recently, we have shown that dithiocarbamate met all the necessary requirements as a precursor for the fabrication of thin films by AACVD.[24] Herein, we identify a new cadmium compound, $Cd[S_2CNCy_2]_2$.py (**1**), and evaluated its potential as a precursor for the fabrication, using AACVD, of pure hexagonal greenockite CdS nanostructured thin films on crystalline FTO and soda glass substrates. The CdS thin films were characterized for their optical and PEC properties. A detailed study of the effect of various deposition parameters, such as solvent, nature of substrate, and deposition temperature on the morphology, particle size, and composition of the films has been undertaken, and summarized.

2. Results and Discussion

The precursor **1** was isolated in 85% yield as a colorless solid from the metathetical reaction of sodium dicyclohexyldithiocarbamate and cadmium(II) nitrate trihydrate from a chloroform-pyridine solution, as shown in the chemical Equation 1.

$$Cd(NO_3)_2 \cdot 3H_2O + 2Na(S_2CN(C_6H_{11})_2) \xrightarrow[\text{chloroform}]{\text{Pyridine}} Cd[(S_2CN(C_6H_{11})_2)_2(C_5H_5N)] + 2NaNO_3 + 3H_2O \quad (1)$$

Precursor **1** has been characterized by elemental analysis, infra red (IR), thermogravimetry (TG), and single-crystal XRD analysis. The IR spectra of dithiocarbamate complexes contain three main regions of interest: The 1580–1450 cm^{-1} region is mainly related with the stretching of the C−N bond of NCS_2^-; the 1060–940 cm^{-1} region, associated with $\nu(-CS_2)$; and the 420–250 cm^{-1} region, associated with ν(M−S). The strong absorption bands at about 1473 and 1441 cm^{-1} in the IR spectrum of **1** are attributed to the ν(C−N) stretching vibrations. These values lie between the range reported for C−N single bond (1250–1360 cm^{-1}) and C=N double bond (1640–1690 cm^{-1}), indicating the partial double bond character in the C=N bond.[25] The $\nu(CS_2)_{asym}$ and $\nu(CS_2)_{sym}$ vibrations that appear at 1055 cm^{-1} and 961 cm^{-1} in the dithiocarbamate ligand are substituted by a strong singlet at about 997 cm^{-1} in **1**, indicating that the dithiocarbamate moiety is symmetrically coordinated to the metal ions.[26]

2.1. Single Crystal X-Ray Analysis

The binary metal dithiocarbamate of the zinc-triad elements, as well their 1,1-dithiolate analogues, e.g., xanthate and dithiophosphate, are well known to aggregate in the solid-state via M.S secondary interactions to form higher dimensional aggregates.[27] Directly relevant to the present study is the centrosymmetric dinuclear structural motif of $\{Cd(S_2CNR_2)\}_2$, uniformly adopted by structures of this formulation.[27] In this motif, one sulfur atom of one of the two chelating dithiocarbamate ligands bridges a cadmium atom so that each cadmium is five-coordinate. It is also well known that the addition of a Lewis base disrupts the structural motif of the original binary species giving rise to structures of lower dimensionality and/or nuclearity.[28,29] In the case of $Cd[S_2CNCy_2]_2$, the addition of pyridine results in the formation of the 1:1 adduct, $Cd[S_2CNCy_2]_2$.py (**1**). The molecular structure is shown in Figure 1. The crystal data and structure refinement details and geometric parameters are collected in Tables 1 and 2, respectively. Figure 1 shows that the cadmium atom is in a five-coordinate NS_4 coordination geometry defined by chelating dithiocarbamate ligands and the pyridine-N atom. It is noted that the dithiocarbamate ligands form slightly asymmetric bonds, as reflected in the values of $\Delta(Cd-S) = 0.065$ and 0.058 Å for the S1- and S3-containing ligands, respectively; the range of Cd−S bond distances is 2.5683(7) to 2.6518(6) Å. The dihedral angle between the chelate rings is 45.28(6)°, and the dihedral angles between these and the pyridine ring are 62.42(9)° and 76.07(9)°, indicating a twist in the relative orientation of the pyridine ring to the chelate rings.

 © 2012 WILEY-VCH Verlag GmbH & Co. KGaA, Weinheim

Chemical Vapor Deposition

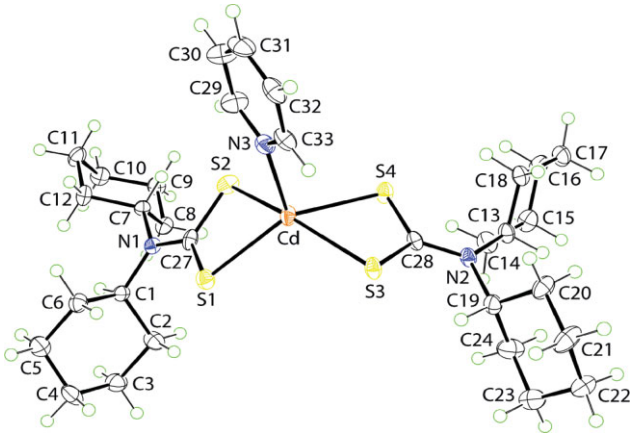

Fig. 1. Molecular structure of **1**. Displacement ellipsoids are drawn at the 50% probability level. Only one orientation of the disordered NCy_2 residue is shown for reasons of clarity.

The geometry of **1** is distorted with a tendency towards square pyramidal. This is quantified by the value of τ [30] of 0.28, which is nearer to an ideal square pyramidal geometry ($\tau = 0$) than to an ideal trigonal bipyramidal geometry with $\tau = 1.0$. Not surprisingly, given the steric bulk of the cyclohexyl rings in **1**, there is limited supramolecular aggregation in the crystal structure, Figure 2. Centrosymmetrically related molecules are connected into dimeric aggregates via S.S interactions involving S3 atoms.[31] Supramolecular chains are formed along the *a*-axis whereby the dimeric aggregates thus formed are connected via C–H. π interactions,[31] where the π–system is a chelate ring. Such interactions are recognized as being important contributors to the stabilization of the crystal structures of metal dithiocarbamates.[32]

Table 1. Crystal data and structure refinement for precursor **1**.

Formula	$C_{31}H_{49}CdN_3S_4$
Formula weight	704.37
Crystal system	triclinic
Space group	$P\bar{1}$
a [Å]	8.9806(4)
b [Å]	13.2878(5)
c [Å]	14.5560(6)
α [°]	76.977(3)
β [°]	85.652(4)
β [°]	82.914(4)
V [Å^3]	1677.33(12)
Z	2
μ [cm^{-1}]	0.925
D_x [g cm^{-3}]	1.395
No. independent reflections	7603
No obs. reflections with $I > 2\sigma(I)$	6401
R (obs. data)	0.033
a in weighting scheme	0.032
Rw (all data)	0.078
CCDC No.[a]	851624

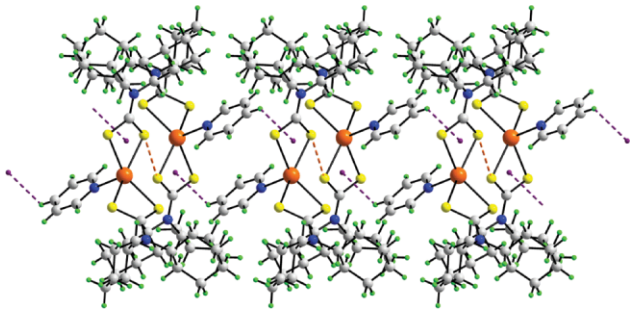

Fig. 2. A view of the supramolecular chain in the crystal structure of **1**. The chains are sustained by S.S and C–H. π (chelate) interactions, shown as orange and purple dashed lines, respectively.

2.2. Thermal Studies

The thermal characteristics of **1** have been examined by thermogravimetric analysis (TGA), performed at a heating rate of 5 °C min^{-1} under an inert atmosphere of nitrogen gas flowing at 25 mL min^{-1}. The TG curve (Fig. 3) shows that the overall pyrolysis of **1** was accomplished in three complex phases. The first phase ranges from 80 to 123 °C, causing a mass loss of 9.67%, indicating partial elimination of a total of 11.21% of pyridine. Following this step is the second broad and weak phase in the temperature limits of 123–275 °C, yielding a mass loss of 7.45%. The third and the last decomposition stage, that ranges from 275 to 350 °C, releases the major mass loss of 61.50%, resulting in a stable residual amount of 21.39% of the initial mass of **1**. This residual mass is close to the expected 20.30% mass for CdS, indicating that **1** has decomposed quantitatively into cadmium sulfide phase. Differential (D)TG also confirms the existence of three phases of decomposition of **1** and indicates temperatures of maximum heat intake at 108, 207, and 339 °C in each degradation stage, respectively.

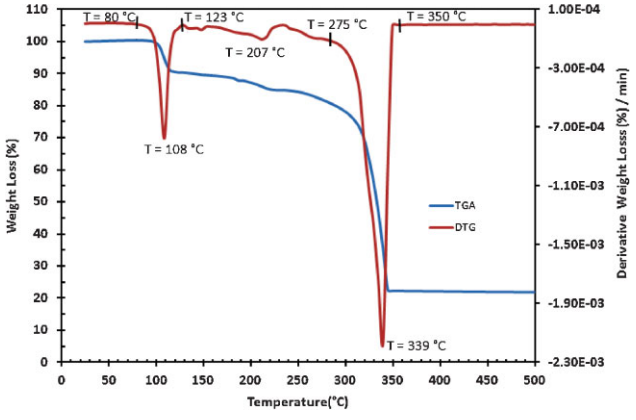

Fig. 3. TGA/DTG plots showing losses in mass with increase in temperature for precursor **1**.

 © 2012 WILEY-VCH Verlag GmbH & Co. KGaA, Weinheim

2.3. Deposition and Characterization of Greenockite Thin Films

Thin films from **1** were grown on crystalline FTO glass and amorphous soda glass substrates under a dynamic argon flow of 100 mL min^{-1} using pyridine, toluene, and THF as solvents at deposition temperatures of 350, 400, and 450 °C. A comparison of the XRD patterns of the thin films grown in pyridine (Figs. 4a,b) and THF (Figs. 4c,d) on FTO and soda glass substrates with standard CdS [00-001-0780][33] revealed that the crystalline product formed is pure CdS ''greenockite'' in its hexagonal modification that crystallized in the *P*63*mc* space group. The calculated values of hexagonal lattice constants are found to be $a = b = 4.1420$ Å and $c = 6.7240$ Å, which agrees well with the standard values for CdS [00-001-0780]. It is observed that as the substrate temperature increases, the intensity and sharpness of peaks also increases due to the improvement in crystallinity without affecting the hexagonal CdS phase. The diffraction patterns of CdS on soda glass (Fig. 4b), however, exhibit some preferred orientations (002) with higher peak intensity when compared to the films deposited on FTO (Fig. 4a) from pyridine. These XRD peak patterns show no signs of any chemically or pyrolytically driven impurity phases of elemental cadmium, sulfur, and CdO. This observation is in contrast to an earlier study where films deposited from the precursor Cd[{(SP^{i}Pr$_2$)$_2$N}$_2$] using AACVD[20] and low-pressure (LP)CVD[5] were highly dependent on temperature, and were contaminated with traces of phosphorous. Interestingly, the use of **1** in the deposition of thin films from various solvents and temperatures consistently produced the hexagonal phase of deposited CdS. In another report, CdS thin films deposited through fluid deposition techniques from the precursor [Cd(S$_2$CN(Hexyl)$_2$)$_2$] yielded sulfur-deficient CdS thin films, and an extra sulfur source was employed to balance the stoichiometry.[34]

Table 2. Selected bond lengths [Å] and angles [°] for precursor **1**.

Bond distances [Å]	
Cd–S1	2.5683(7)
Cd–S2	2.6333(6)
Cd–S3	2.5941(6)
Cd–S4	2.6518(6)
Cd–N3	2.311(2)
Bond angles [°]	
S1–Cd–S2	69.14(2)
S3–Cd–S4	68.251(18)
S1–Cd–S3	109.65(2)
S1–Cd–S4	138.42(2)
S2–Cd–S3	155.43(2)
S2–Cd–S4	95.954(19)

2.4. AACVD and SEM/EDX Studies

The architecture of thin films deposited by AACVD depends on gas-phase nucleation of homogeneous and heterogeneous reactions, and is influenced by the deposition

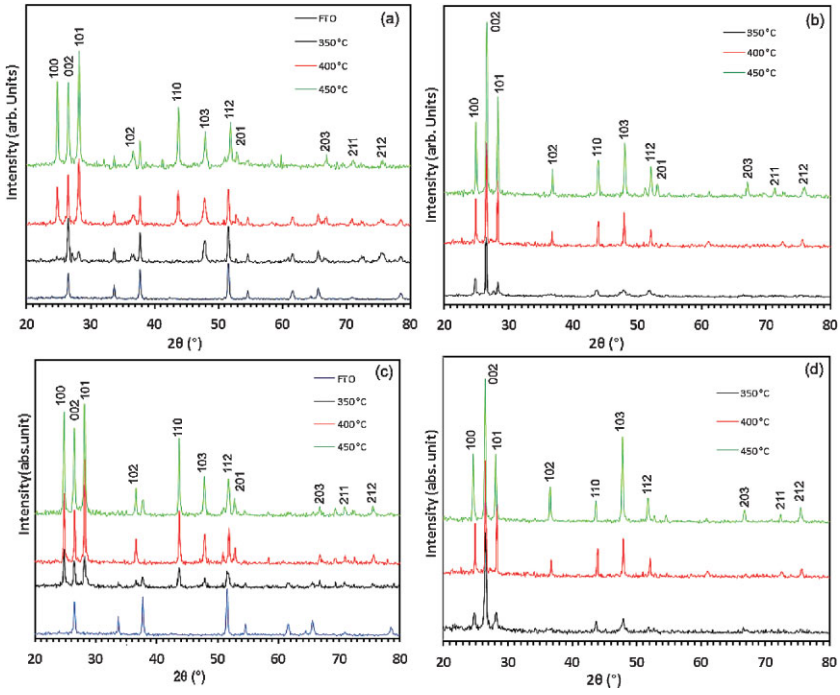

Fig. 4. XRD patterns of greenockite CdS thin films deposited from **1** on substrates (a) FTO, (b) soda glass using pyridine; (c) FTO, (d) soda glass via THF solutions at 350, 400, and 450 °C, respectively.

 © 2012 WILEY-VCH Verlag GmbH & Co. KGaA, Weinheim

Table 3. Effect of nature of substrate, solvent, and temperature on morphology, particle size and elemental ratio of greenockite (CdS) thin films deposited from **1**.

Figure no.	Solvent type	Substrate	Substrate temperature [°C]	Crystallite morphology	Particle size [nm]	Elemental ratio [Cd:S]
5(a)	Pyridine	FTO	350	hexagon	250	0.98:1.02
(b)	Pyridine	FTO	400	distorted hexagon	180	0.99:1.01
(c)	Pyridine	FTO	450	corn grain	220	1.04:0.96
(d)	Pyridine	Soda glass	350	cauliflower	>1000	0.99:1.01
(e)	Pyridine	Soda glass	400	round grain	150–200	1.00:1.00
(f)	Pyridine	Soda glass	450	snowflake	250–300	1.04:0.96
6(a)	Toluene	FTO	350	rough hexagon	300	0.90:1.10
(b)	Toluene	FTO	400	hexagonal sheet	350	0.88:1.12
(c)	Toluene	FTO	450	flake	180–540	0.94:1.06
(d)	Toluene	Soda glass	350	agglomerate heap	250–500	0.97:1.03
(e)	Toluene	Soda glass	400	flake	540–720	0.90:1.10
(f)	Toluene	Soda glass	450	flake	>1000	1.04:0.96
7(a)	THF	FTO	350	stripe	55	0.98:1.02
(b)	THF	FTO	400	crumbled particle	100	0.95:1.05
(c)	THF	FTO	450	flake	200–400	1.07:0.93
(d)	THF	Soda glass	350	irregular grain	300–400	1.02:0.98
(e)	THF	Soda glass	400	heap	>1000	1.04:0.96
(f)	THF	Soda glass	450	flake	>1000	1.01:0.99

conditions, such as the physical properties of the solvent (boiling point, heat of combustion, viscosity, specific heat capacity, and coordination ability), as well as the growth temperature and nature of the substrate. By tuning these parameters, greenockite thin films with a variety of morphologies, mutable particle size, and composition have been engineered and these features are summarized in Table 3. FESEM images of the films deposited from **1** on FTO and soda glass substrates at 350, 400, and 450 °C using pyridine, toluene, and THF as solvents are shown in Figures 5, 6 and 7, When films were deposited in the temperature range 350–450 °C using pyridine solution, different morphologies were detected on FTO and soda glass substrates. At 350 °C, regular-shaped hexagons of size 250 nm, tightly coupled with each other, manifested clear boundaries and edges on the FTO glass. Similar hexagonal CdS nanocrystals have been prepared earlier by solution methods.[35] On increasing the temperature to 400 °C, the hexagonal geometry starts to deteriorate to small-sized 180 nm particles (Fig. 5b) and, at 450 °C, completely converted to isolated corn grains having particle size of 220 nm (Fig. 5c).

Various greenockite nanostructures were obtained when FTO glass was replaced by a soda glass substrate

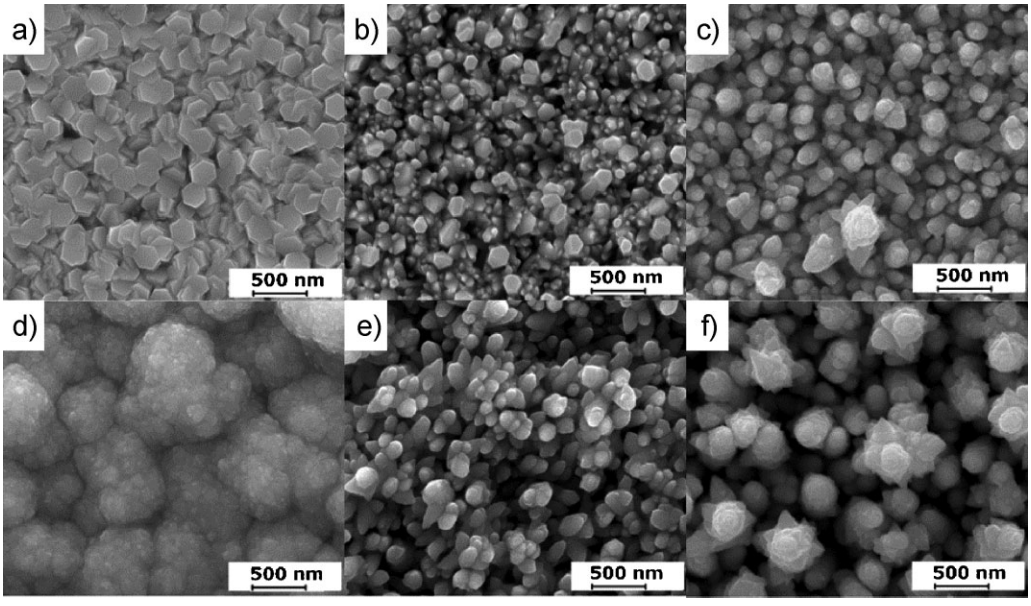

Fig. 5. SEM images of greenockite(CdS) thin films deposited from **1** on FTO (a–c) and soda glass (d–f) at 350, 400, and 450 °C in pyridine solution, respectively.

 © 2012 WILEY-VCH Verlag GmbH & Co. KGaA, Weinheim

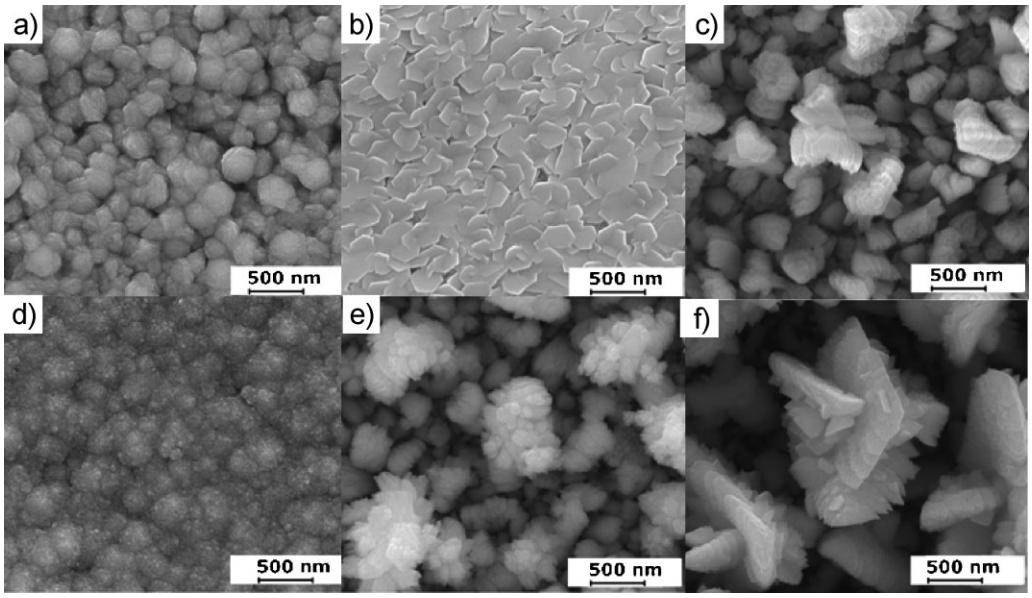

Fig. 6. SEM images of greenockite (CdS) thin films deposited from **1** on FTO (a–c) and soda glass (d–f) at 350, 400, and 450 °C in toluene solution, respectively.

(Figs. 5d–f). At 350 °C, tightly bound, spherical, cauliflower-like architectures of size >1 μm (Fig. 5d), made from a combination of several small particles of size 30–50 nm, were formed. On further increasing the temperature to 400 °C, round-shaped particles of size 150–200 nm, growing in a perpendicular direction, were obtained. At 450 °C, the growth direction along the perpendicular axis continued to produce large, intergrown white flakes of size 250–300 nm (Fig. 5f).

Thin films deposited from a toluene solution of **1** indicate some growth of hexagonal crystallite of average size 300 nm on FTO glass at 350 °C (Fig. 6a). At 400 °C, randomly oriented but interconnected hexagonal plates of average size 350 nm became visible. With a further increase in temperature to 450 °C, a morphology shift was apparent in that small and large-sized flakes, ranging from 180 to 540 nm were noted.

When deposition experiments under similar conditions were carried out on a soda glass substrate, irregular-shaped small heaps appeared at 350 °C (Fig. 6d). On further increase in temperature to 400 °C, flake-like objects of size 540–720 nm started growing; these later converted to large, intergrown flakes in the size range >1 μm at 450 °C (Fig. 6f).

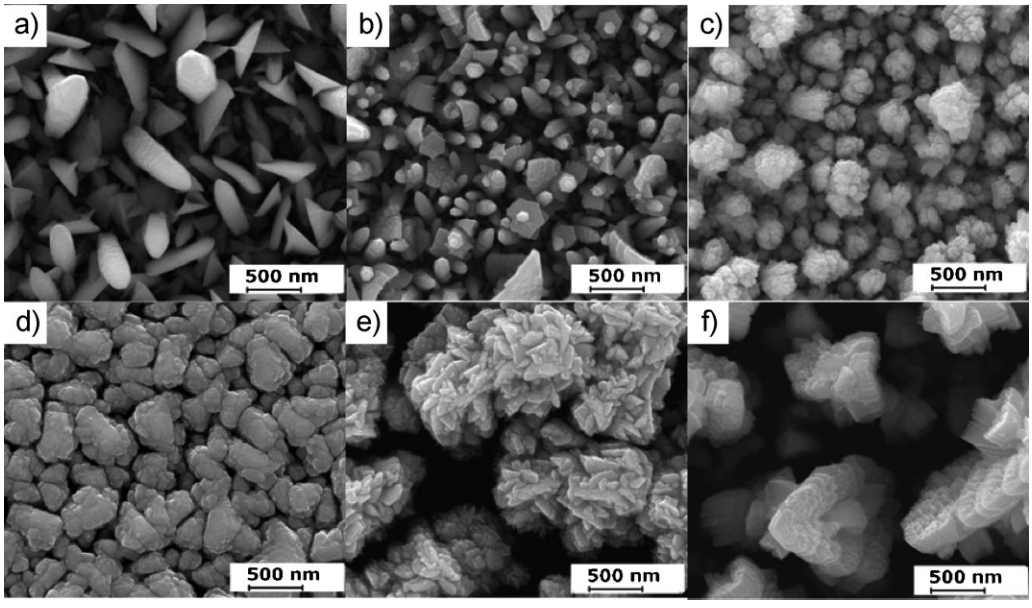

Fig. 7. SEM images of greenockite (CdS) thin films deposited from **1** on FTO (a–c) and soda glass (d–f) at 350, 400, and 450 °C from THF solution, respectively.

 © 2012 WILEY-VCH Verlag GmbH & Co. KGaA, Weinheim

The effect of solvent on greenockite nanostructures, morphology, and composition in THF was also studied on FTO (Figs. 7a–c) and soda glass substrates (Figs. 7 d–f).

At 350 °C, growths of strip-like objects of varying length and breadth, with clear texture and boundaries, were bred without any directional preferences. At 400 °C, these strips started caving down to small objects of size ca. 100 nm, as shown in Figure 7b, and at 450 °C agglomeration of small particles (50 nm) took place to furnish large heaps of sizes 200–400 nm. The fabrication of thin films on soda glass, as shown in Figures 7d–f, under similar conditions except for temperature variation, also revealed changes in morphology. At 350 °C, irregular grains of size 300–400 nm with distinct boundaries appeared, and these changed into heaps of large sizes >2 μm at 400 °C. At 450 °C, considerably interconnected flakes of different sizes appeared (Fig. 7f).

Depending on the temperature of the deposition chamber, the aerosol droplets undergo evaporation, vaporization, precipitation, and thermolysis before or after reaching the substrate surface. We believe that, at relatively low temperatures, the heterogeneous process is dominant and the precursor molecule adsorbed on the substrate surface, and subsequent evaporation, vaporization, and decomposition tends to produce high-quality, designed films with good adhesive strength (Figs. 5a, 6b, 7a). With the increase in temperature to 400 °C, the aerosol absorbs more heat in the delivery tube causing solvent evaporation, while vaporization of precursor molecules starts before adsorbing on the substrate surface, which results in the deposition of films with a distorted structure (Figs. 5b, 6b). With a further increase in temperatures to 450 °C, the temperature gradient inside the delivery tube reached the flash point of the solvent. This leads to the burning and decomposition of the solvent, causing evaporation, vaporization, precipitation, and thermolysis of aerosol droplets in a single-step in the gas phase. This process is brought about by the mechanism of heat and mass transfer inside the droplets, and between the droplets and surrounding gas, resulting in the formation of thin films governed by the homogeneous deposition process. Such a mechanism enables high decomposition as well as segregation suppression to the droplet scale, resulting in the formation of nanometer-scale particles in the gas phase. These nanometer-scale particles adsorb on the substrate surface, and act as nuclei for the further growth of porous thin film with irregular texture and poor adhesion to the substrate (Figs. 5c, 6c, 7c).

The role of solvent in the building of robust nanostructures (Figs. 5a, 6b, 7a) can be described on the basis of heat of combustion[2] and the coordinating ability of the solvent. Pyridine, having moderate heat of combustion (2782 kJ mol^{-1}) and high coordinating ability, favors heterogeneous nucleation mode at 350 °C, while toluene, with much higher heat of combustion (3910.3 kJ mol^{-1}) and having no coordinating ability, facilitates both the homogeneous and heterogeneous nucleation at 400 °C. In contrast, THF with much lower heat of combustion (2501.2 kJ mol^{-1}) when compared to both pyridine and toluene, evaporates faster causing homogeneous nucleation at 350 °C.

It is noteworthy that selective nanostructures were only produced by conducting FTO substrate where the landing of a charged aerosol cluster is a function of the electrical and electrochemical nature of the conducting substrate which is more favorable to nucleation than insulating soda glass. When a charged aerosol droplet undergoes evaporation, the electric charge density increases with the shrinking of the droplet, and the conducting substrate offers intense repulsion which splits the particle apart until the solvent completely evaporates.[36] As a result, multiple fine particles are selectively formed and adsorbed on the conducting substrate, where a specific ripening and growing process yields the selective structures (Figs. 5a, 6b, 7a).

All deposition experiments carried out in the solvents pyridine, toluene, and THF led to the fabrication of yellow greenockite CdS thin films at 350 and 400 °C that adhered well to both the FTO and soda glass substrates, and passed the ''scotch tape test'', while the films deposited at 450 °C show a change in color from bright-yellow to dark-yellow brown, became less adherent to the substrates, and failed the scotch tape test.

2.5. Optical Properties

The UV-vis spectra of the greenockite thin films in the wavelength range of 350–900 nm, using SnO_2 as a reference, were recorded to calculate the band gap (E_g) from the Tauc plot as given by the formula $\alpha h\nu = A_0(h\nu - E_g)^n$ (where A is a constant, and n is the power of the exponent) which takes a value of 1/2 for directly allowed and 2 for indirectly allowed transitions; E_g is the band gap and $h\nu$ is the incident photon energy. It is possible to determine the nature of the transitions by plotting graphs of $(\alpha h\nu)^n$ versus $h\nu$ for different values of ''n''. It has been observed that the UV-vis data of greenockite thin films prepared in pyridine, in the temperature range 350–450 °C, fitted very well to $n = 2$ (Fig. 8). The band gap is estimated from the intercept of the extrapolated linear fit to the experimental data of the Tauc plot. A band gap of 2.4 eV was estimated by this procedure, as shown in Figure 8 (inset). It has been observed that the E_g of CdS was not significantly affected by deposition temperature, and that the estimated band gaps were found to be very close to reported values for other CdS thin films.[37]

2.6. PEC Studies

Based on nanostructure, morphology, and compactness, greenockite thin film electrodes prepared from pyridine solution at 350, 400, and 450 °C were tested for their PEC properties in a three-electrode mode using an aqueous 0.1 M

 © 2012 WILEY-VCH Verlag GmbH & Co. KGaA, Weinheim

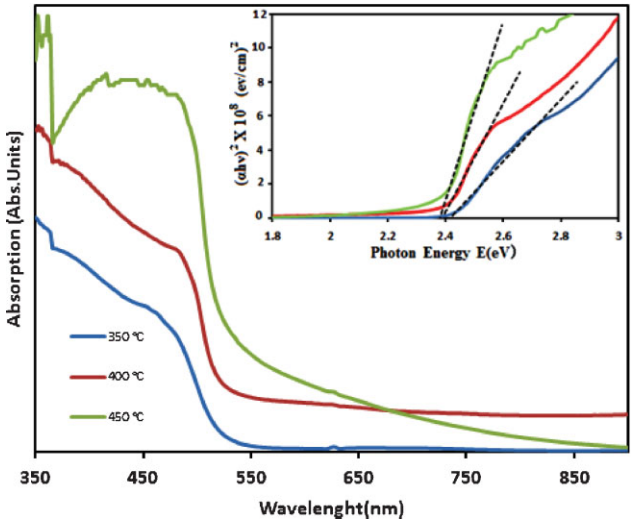

Fig. 8. Optical absorption spectrum of greenockite (CdS) thin films deposited from precursor **1**. Inset: Tauc plot showing the estimated optical band gap of 2.4.

Na_2SO_3 solution as an electrolyte. The *J–V* plots of all the three thin film electrodes are shown in Figure 9. The nanocrystalline greenockite photoelectrodes prepared at 350, 400, and 450 °C showed photocurrent densities at 0.4 V of 1.3, 1.0, and 0.6 mA cm^{-2}, respectively, vs. Ag/AgCl/3M KCl. It is noted that the photocurrent density significantly depends on the nanostructure and architecture of the photoelectrode that, in turn, alters with the deposition temperature. At 350 °C, tightly interconnected hexagons (Fig. 5a) increase light residence time, reduce reflectivity, and increase charge mobility to provide a good path for the excitation of electron-holes, correlating nicely with the observed maximum photocurrent density. With the increase in the substrate deposition temperature, the ordered hexagonal structure partly deteriorates into small particles, resulting in defects and voids in the nanocrystalline structure

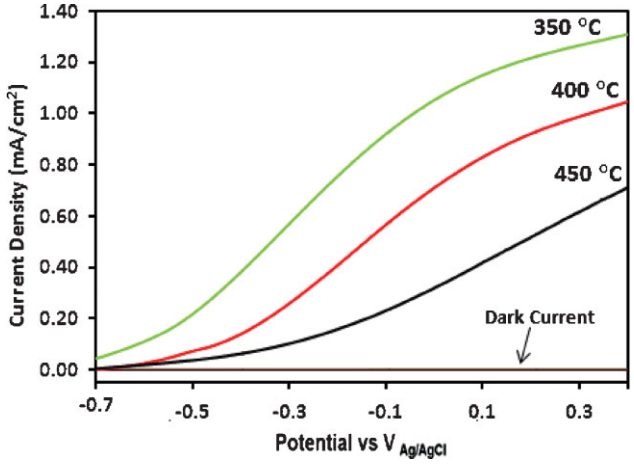

Fig. 9. *J – V* curves for the greenockite (CdS) thin film electrodes deposited from **1** in pyridine measured under simulated AM 1.5 sunlight in aqueous 0.1M Na_2SO_3 solution as an electrolyte.

that may act as recombination centers for the photogenerated electron-hole pairs, and consequently show poor PEC performance. Similarly, at 450 °C the premature precursor decomposition and nucleation produces loosely bonded films, thereby influencing the morphology and texture, and thus diminishing the photocurrent density.

3. Conclusions

In summary, various architectures of impurity-free nanocrystalline greenockite (CdS) can be grown, using AACVD, from an easily synthesizable, single-source precursor, $Cd[S_2CNCy_2]_2.py$ (**1**), in solutions of pyridine, toluene, and THF, in the temperature range of 350 –450 °C, on FTO and soda glass substrates. The XRD, FESEM, and EDX analyses of the thin films confirm the formation of nanocrystalline greenockite, with well-defined morphologies and precise elemental ratios. The PEC studies carried out on hexagonal films deposited on FTO at 350 °C from pyridine solution exhibit a photocurrent density of 1.3 mA cm^{-2} at 0.4 V versus Ag/AgCl/3M KCl, while films deposited at 400 and 450 °C under similar conditions show inferior PEC performance. Thus, by manipulating the deposition conditions, thin films of diverse nanostructures and architectures can be fabricated for technological applications.

4. Experimental

All reactions were carried out at room temperature. Reagent grade solvents were used without further purification. All starting materials were purchased from Sigma Aldrich and used without further purification. The sodium dicyclohexyldithiocarbamate ligand was produced by the reaction of dicyclohexyl amine with CS_2 in the presence of NaOH in chloroform, and crystallized from the same solvent. Elemental analysis was performed using a Leco CHNS 932. Infrared spectra were recorded with a Perkin Elmer Spectrum 400 FT-IR/FT-FIR spectrophotometer. The controlled thermal analysis was investigated using a METTLER TOLEDO TGA/SDTA 851e Thermogravimetric Analyzer with a computer interface. The thermal measurements were carried out in an alumina crucible under an atmosphere of flowing nitrogen gas (25 mL min^{-1}) with a heating rate of 5 °C min^{-1}.

*4.1. Synthesis of $Cd[S_2CNCy_2]_2.py$ (**1**)*: Sodium dicyclohexyldithiocarbamte (2.00 g, 7.16 mmol) was dissolved in chloroform (25 mL) and placed in a 250 mL round bottom flask fitted with a dropping funnel, reflux condenser, and inert gas line. $Cd(NO_3)_2 \cdot 3H_2O$ (1.10 g, 3.58 mmol) was added, and the milky white solution was stirred for 30 min. At this point, 30 mL pyridine was added to give a clear and colorless solution, and stirring was continued for a further one hour. Filtration and slow evaporation of the reaction mixture afforded precursor **1** as colorless crystals. Yield 85%. Decomposition pt. 220 °C. Analysis: Calculated for $C_{31}H_{49}CdN_3S_4$: calcd. C 52.81, H 6.95, N 5.96, S 18.17; found C 50.92, H 6.679, N 6.368, S 18.07%. IR (cm^{-1}): 1474 s, 1441 s [ν(C–N)]; 997s [ν(C–S)]; ^{1}HNMR (399.1 MHz,$CDCl_3$): $\delta = 1.13$ –3.21 ppm [complex pattern, 44H,] 7.32 –8.67 ppm [5H, aromatic]. TGA: Mass loss 89 –123 °C, 9.67%; 128 –270 °C, 7.45%; 271 –349 °C, 21.39% residue.

4.2. X-ray Crystallography: Intensity data for precursor **1** were measured at 100 K on an Agilent SuperNova Dual diffractometer with Atlas detector [38], fitted with Mo Kα radiation, so that θ_{max} was 27.5°. The structure was solved by heavy-atom methods (SHELXS97) [39] and refinement was on F^2 (SHELXL97) [40] using data that had been corrected for absorption effects with an empirical procedure [39] with non-hydrogen atoms modeled with anisotropic displacement parameters, with hydrogen atoms in their calculated positions, and using a weighting scheme of the form $w = 1/[\sigma^2(F_o^2) + (aP)^2]$ where $P = (F_o^2 + 2F_c^2)/3$). Disorder was resolved for the

 © 2012 WILEY-VCH Verlag GmbH & Co. KGaA, Weinheim

NCy_2 residue rings of one dithiocarbamate ligand in **1** so that two distinct positions were determined for each atom. Refinement showed that each component had a similar site occupancy factor, so this was fixed at 0.5 in the final cycles of refinement. Chemically equivalent atoms were assigned equivalent anisotropic displacement parameters, and the fragments were refined with soft constraints using the SADI, ISOR, and DFIX commands in SHELX97 [40]. Finally, two reflections, i.e. $\bar{1}$ 3 2) and (4 -6 7), were omitted from the final cycles of refinement owing to poor agreement. The molecular structure of **1** is shown in Figure 1, which was generated with ORTEP-3 [40] at the 50% probability level; Figure 2 was drawn with DIAMOND using arbitrary ellipsoids [41]. Data analyses were performed with WinGX [42] and PLATON [43]. Crystallographic data and refinement details are given in Table 1.

4.3. Deposition of Thin Films by AACVD: Thin films from **1** were deposited on commercially available soda glass and FTO coated glass (1 cm × 2 cm) slides (TEC 15, 12 ~ 14 Ω/sq) by using an in-house, ultrasonic, AACVD assembly as described elsewhere [22]. The FTO and soda glass substrates were ultrasonically cleaned before use in distilled water, isopropanol, and acetone, and were finally stored in ethanol. In a typical deposition, a 0.05 M solution of **1** in various solvents was used to generate the aerosol at room temperature using an ultrasonic air humidifier operating at 50 Hz frequency. Argon gas was passed through the aerosol mist at a flow rate of 100 mL min^{-1} to force aerosol droplets into the reactor chamber. Depositions were conducted for 35 min. The exhausts from the reactor was vented directly into the extraction system of a fume cupboard. Towards the end of the experiment, the aerosol line was closed, and argon was allowed to flow over the substrate. The films were cooled to 40 °C before they were removed from the reaction chamber for structural and PEC studies. Several AACVD experiments under similar conditions were undertaken to ensure the reproducibility of the generated thin films.

4.4. Structural Characterization: The identity of the phase and the degree of crystallinity of the deposited films were investigated using a PANalytical X-ray diffractometer model X'Pert PRO with primary monochromatic high intensity Cu Kα (λ = 1.54184 Å) radiation in the 2θ range 5.00 to 80.00°. Data on the morphology and composition of the thin films were obtained using FESEM (FEI Quanta 400) coupled with an EDX spectrometer, GENESIS.

4.5. Optical and PEC Characterization: Room temperature UV-vis absorption spectra were recorded on a Lambda 35 Perkin-Elmer UV-vis spectrophotometer in the wavelength range 300–900 nm using a similar FTO-coated glass substrate as a reference. Thus, the reported absorbance spectra included the contributions from the greenockite films only. A three-electrode electrochemical cell fitted with a quartz window was used for PEC characterization, and an aqueous solution 0.1M Na_2SO_3 was used as the electrolyte The potential of the greenockite working electrodes was controlled by an Autolab (302N) Potentiostat/Galvanostat instrument. An Ag/AgCl/3M KCl electrode was used as the reference electrode and a Pt wire was adopted as the counter electrode, while the illumination source was an AM1.5 class A solar simulator (Solar Light 16S–300 solar simulator) with a voltage scan speed of 10 mV s^{-1}.

4.6. Supporting Information: CCDC-851624 contains the supplementary crystallographic data for this paper. The data can be obtained free of charge from the Cambridge Crystallographic Data Centre via www.ccdc.cam.ac.uk/data_request.cif.

Received: March 2, 2012
Revised: April 11, 2012

[1] D. Kaushik, R. R. Singh, M. Sharma, D. K. Gupta, N. P. Lalla, R. K. Pandey, *Thin Solid Films* **2007**, *515*, 7070.

[2] A. A. Tahir, K. G. U. Wijayantha, *J. Photochem. Photobiol. A–Chem.* **2010**, *216*, 119.

[3] F. E. Osterloh, *Chem. Mater.* **2008**, *20*, 35.

[4] A. A. Yadav, E. U. Masumdar, *J. Alloy Compd.* **2011**, *509*, 5394.

[5] M. Afzaal, D. Crouch, M. A. Malik, M. Motevalli, P. O'Brien, J.-H. Park, J. D. Woollins, *Eur. J. Inorg. Chem.* **2004,** 171.

[6] (a) P. S. Nair, T. Radhakrishnan, N. Revaprasadu, G. A. Kolawole, P. O'Brien, *Chem. Commun.* **2002**, 564. (b) Z. Li, W. Cai, J. Sui, *Nanotechnology* **2008**, *19*, 035602. (c) M. T. Ng, C. Boothroyd, J. J. Vittal, *Chem. Commun.* **2005**, 3820.

[7] (a) N. Pradhan, B. Katz, S. Efrima, *J. Phys. Chem. B* **2003**, *107*, 13843. (b) N. D. Sankir, B. Dogan, *J. Mater. Sci.* **2010**, *45*, 6424.

[8] P. K. M. Bandaranayake, P. V. V. Jayaweera, K. Tennakone, *Sol. Energy Mater. Sol. Cells* **2003**, *76*, 57.

[9] J. N. Ximello-Quiebras, G. Contreras-Puente, J. Aguilar-Hernández, G. Santana-Rodriguez, R. Arias-Carbajal, *Sol. Energy Mater. Sol. Cells* **2004**, *82*, 263.

[10] D. P. Amalnerkar, K. Yamaguchi, T. Kajita, H. Minoura, *Solid State Commun.* **1994**, *90*, 3.

[11] H. Uda, H. Yonezawa, Y. Ohtsubo, M. Kosaka, H. Sonomura, *Sol. Energy Mater. Sol. Cells* **2003**, *75*, 219.

[12] S. Ray, R. Banerjee, A. K. Barua, *J. Appl. Phys.* **1980**, *19*, 1889.

[13] B. S. Moon, J. H. Lee, H. Jung, *Thin Solid Films* **2006**, *511*, 299.

[14] H. M. Manasevit, *J. Cryst. Growth* **1981**, *55*, 1.

[15] N. L. Pickett, P. O'Brien, *Chem. Rec.* **2001**, 467.

[16] P. O'Brien, *Inorganic Materials* (Eds: D. Bruce, D. O'Hare), Wiley, Chichester **1997**, p. 523.

[17] (a) A. Saunders, A. Vecht, G. Tyrell, *Chem. Abs.* **1988**, *108*, 66226h. (b) D. M. Frigo, O. F. Z. Khan, P. O'Brien, *J. Cryst. Growth* **1989**, *96*, 989. (c) M. Chunggaze, M. A. Malik, P. O'Brien, *Adv. Mater. Opt. Electron.* **1997**, *7*, 311.

[18] (a) F.-X. Wei, X. Yin, W.-G. Zhang, J. Fan, X.-H. Jiang, S.-L. Wang, *Z. Kristallogr. NCS* **2005**, *220*, 417. (b) S. M. Zemskova, G. Prashad, L. A. Glinskaya, R. F. Klevtsova, V. B. Durasov, S. V. Tkachev, S. A. Gromilov, S. V. Larionov, *Russ. J. Inorg. Chem.* **1998**, *43*, 1525.

[19] (a) P. V. Subha, P. Valarmathi, N. Srinivasan, S. Thirumaran, K. Saminathan, *Polyhedron* **2010**, *29*, 1078. (b) S. Thirumaran, K. Ramalingam, G. Bocelli, L. Righi, *Polyhedron* **2009**, *28*, 263. (c) B. Arulprakasam, K. Ramalingam, G. Bocelli, A. Cantoni, *Polyhedron* **2007**, *26*, 4489.

[20] D. Oyetunde, M. Afzaal, M. A. Vincent, I. H. Hillier, P. O'Brien, *Inorg. Chem.* **2011**, *50*, 2052.

[21] K. Ramasamy, M. A. Malik, P. O'Brien, J. Raftery, *Dalton Trans.* **2010**, *39*, 1460.

[22] A. A. Tahir, K. G. U. Wijayantha, S. Saremi-Yarahmadi, M. Mazhar, V. McKee, *Chem. Mater.* **2009**, *21*, 3763.

[23] A. A. Tahir, M. Mazhar, M. Hamid, K. G. U. Wijayantha, K. C. Molloy, *Dalton Trans.* **2009,** 3674.

[24] (a) A. A. Tahir, M. A. Ehsan, M. Mazhar, K. G. U. Wijayantha, M. Zeller, A. D. Hunter, *Chem. Mater.* **2010**, *22*, 5084. (b) J. R. Castro, K. C. Molloy, Y. Liu, C. S. Lai, Z. Dong, T. J. White, E. R. T. Tiekink, *J. Mater. Chem.* **2008,** 5399.

[25] J. J. Criado, J. A. L. Aria, B. Marcias, L. R. F. Lago, *Inorg. Chim. Acta* **1992**, *193*, 229.

[26] B. F. G. Johnson, K. H. Al-Obalidi, J. A. McCleverty, *J. Am. Chem. Soc. A* **1969**, *19*, 1668.

[27] E. R. T. Tiekink, *Cryst. Eng. Commun.* **2003**, *5*, 101.

[28] I. Haiduc, D. B. Sowerby, S. F. Lu, *Polyhedron* **1995**, *14*, 3389.

[29] (a) G. Hogarth, *Prog. Inorg. Chem.* **2005**, *53*, 71. (b) E. R. T. Tiekink, I. Haiduc, *Prog. Inorg. Chem.* **2005**, *54*, 127.

[30] A. W. Addison, T. N. Rao, J. Reedijk, J. Van Rijn, G. C. Verschoor, *J. Chem. Soc. Dalton Trans.* **1984**, 1349.

[31] Intermolecular interactions for Cd[S2CNCy2]2.py: S3.S3i=3. 2792 (8) Å for *i*: 1-*x*, 2-*y*, 1-*z*. C31–H31.Cg(CdS3S4C28)ii=2.96 Å; C31.Cg (CdS3S4C28)ii=3.650(3) Å, with angle at H31=130° for *ii*: 2-*x*, 2-*y*, 1-*z*.

[32] E. R. T. Tiekink, J. Zukerman-Schpector, *Chem. Commun.* **2011**, *47*, 6623.

[33] New Jersey Zinc Co., Palmerton, PA, USA, Private Communication, Dana's System of Mineralogy, 7th Ed.

[34] J. Yang, J. R. Hyde, J. W. Wilson, K. Malik, P. J. Sazio, P. O'Brien, M. A. Malik, M. Afzaal, C. Q. Nguyen, M. W. George, S. M. Howdle, D. C. Smith, *Adv. Mater.* **2009**, *21*, 4115.

[35] Y. Cheng, Y. Wang, F. Bao, D. Chen, *J. Phys. Chem. B* **2006**, *110*, 9448.

[36] X. Hou, K.-L. Choy, *Chem. Vap. Deposition* **2006**, *12*, 583.

[37] S. A. Vanalakar, S. S. Mali, R. C. Pawar, N. L. Tarwal, A. V. Moholkar, J. A. Kim, Y. Kwon, J. H. Kim, P. S. Patil, *Electrochim. Acta* **2011**, *56*, 2762.

 © 2012 WILEY-VCH Verlag GmbH & Co. KGaA, Weinheim

[38] Agilent Technologies. *CrysAlis PRO*. Agilent Technologies, Yarnton, Oxfordshire, England, **2010**, 25.
[39] G. M. Sheldrick, *Acta Crystallogr.* **2008**, *A64*, 112.
[40] L. J. Farrugia, *J. Appl. Crystallogr.* **1997**, *30*, 565.
[41] K. Brandenburg, DIAMOND. Crystal Impact GbR, Bonn, Germany, **2006**.
[42] L. J. Farrugia, *J. Appl. Cryst*, **1999**, *32*, 837.
[43] A. L. Spek, *J. Appl. Crystallogr.* **2003**, *36*, 7.

 © 2012 WILEY-VCH Verlag GmbH & Co. KGaA, Weinheim